THE JOURNAL OF PHYSICAL CHEMISTRY Letters

Perspective

pubs.acs.org/JPCL

Chemically Engraving Semiconductor Nanowires: Using Three-Dimensional Nanoscale Morphology to Encode Functionality from the Bottom Up

Joseph D. Christesen, Christopher W. Pinion, David J. Hill, Seokhyoung Kim, and James F. Cahoon*

Department of Chemistry, University of North Carolina at Chapel Hill, Chapel Hill, North Carolina 27599-3290, United States

ABSTRACT: The patterning of semiconductors with nanometer-scale precision is a cornerstone of modern technology. Top-down methods, ranging from photolithography to focused-ion beam milling, are typically used to fabricate complex nanostructures. In this Perspective, we discuss an alternative bottom-up method to encode similar high-resolution morphology in semiconductor nanowires (NWs). This process, termed ENGRAVE for "Encoded Nanowire GRowth and Appearance through VLS and Etching", combines fast modulation of nanowire composition during vapor−liquid−solid (VLS) growth with composition-dependent wet-chemical etching. This method produces cylindrically symmetric structures in which the diameter is modulated on a sub-10 nm axial length scale. The process can produce patterns that range from periodic, centrosymmetric to nonperiodic, asymmetric structures, including gratings, fractals, tapers, ratchets, sinusoids, nanogaps, and nanodots. We discuss the prospect for the ENGRAVE process to become a complementary method of lithographic-like patterning that encodes unique morphologies and physical properties in semiconductors for a range of technologies.

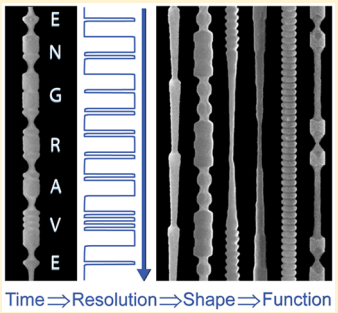

Lithographic tools that can pattern semiconductor materials on length scales from micrometers to nanometers have helped usher in the modern electronic age. The patterning of silicon (Si), in particular, forms the basis for technologies ranging from transistors in computers to motion sensors in smartphones. Si is still a leading material for the development of new technologies such as nanophotonics[1,2] and optomechanics.[3,4] Continued progress with these technologies will require the patterning of progressively higher-resolution and higher-fidelity morphological features. Improvements to lithographic techniques often require the trade-off of high cost (e.g., phase-shift and immersion lithography) and/or low throughput (e.g., electron-beam and focused ion-beam lithographies).[5−7] As a result, bottom-up routes for "chemical nanofabrication" are an attractive alternative to lithographic methods (Figure 1). Nonlithographic methods of generating nanostructures, however, often result in thermodynamically metastable morphologies such as spheres, cubes, cylinders, and nanorods, and the ability to encode arbitrary, high-resolution morphology is often elusive.[8−10]

The nanowire (NW) geometry offers a platform for nanometer-scale morphological control, and significant research effort has been devoted toward controlling the morphology of wires grown by the vapor−liquid−solid (VLS) mechanism.[11−23] For example, the Gradečak research group at MIT modulated the diameter of III−V NW catalysts by altering the catalyst supersaturation, allowing an ∼25% modulation of the NW diameter (Figure 2A) during VLS growth.[14] Because the morphology change is fundamentally linked to the VLS growth mechanism, the results could potentially be generalized to other VLS-grown NW systems. The Filler group at Georgia Tech has developed methods to modulate the surface chemistry of NWs during growth,[13,17] allowing control of vapor−solid sidewall deposition. This method has created tear drop structures in Ge NWs (Figure 2B) by modulating the flow of methyl-containing precursors, which passivate the NW sidewall and prevent deposition. The Lieber group at Harvard University used a high-temperature deposition step following VLS growth to induce the growth of a shell that exhibits Plateau−Raleigh instability (Figure 2C).[12] By altering the temperature and pressures during this growth process, they created a wide variety of periodic structures with control over both the period and cross-sectional profile. The Tian group at the University of Chicago has utilized rapid depressurization during Si NW growth to induce Au deposition and diffusion along the NW axis, which forms a Au silicide that acts as a mask for ex-situ wet-chemical KOH etching.[11] The etch reveals a sawtooth morphology in Si NWs (Figure 2D), which were used as novel atomic force microscopy (AFM) tips for interaction with soft matter. The Samuelson group at Lund University has shown several methods of control over the morphology of III−V NWs. With GaP−GaAs NWs, they have produced gaps through an ex-situ wet-chemical etch to selectively remove the GaAs segments (Figure 2E).[18] For InP NWs, they created long-range twinning super lattices that remove the cylindrical cross section common to many NW systems (Figure 2F).[23] Beyond VLS-grown NWs, the Mirkin group at Northwestern University developed a method termed on-wire lithography (OWL) for creating nanometer-sized gaps in metal NWs (Figure 2G).[24] The NWs are grown via electro-

Received: November 2, 2015
Accepted: January 28, 2016
Published: January 28, 2016

DOI: 10.1021/acs.jpclett.5b02444
J. Phys. Chem. Lett. 2016, 7, 685−692

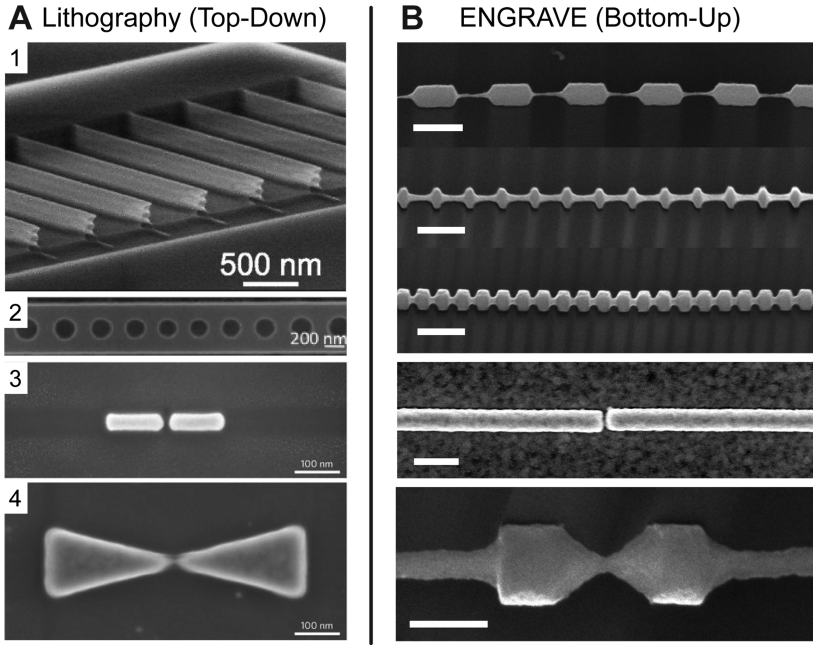

Figure 1. Comparison of top-down lithographic structures and bottom-up ENGRAVE NWs. (A) Top-down lithographic structures, including (1) template-assisted selective epitaxy of stacked NWs, (2) one-dimensional Si photonic crystals, (3) plasmonic antennae, and (4) plasmonic bow-ties. Image 1 reprinted with permission from ref 26. Copyright 2015 AIP Publishing LLC. Image 2 reprinted with permission from ref 6. Copyright 2009 AIP Publishing LLC. Images 3 and 4 adapted by permission from ref 5. Copyright 2011 Macmillan Publishers Ltd. (B) Complementary structures created via bottom ENGRAVE NWs. Top 4 scale bars are 200 nm and bottom scale bar is 100 nm. Images adapted from ref 27. Copyright 2013 American Chemical Society.

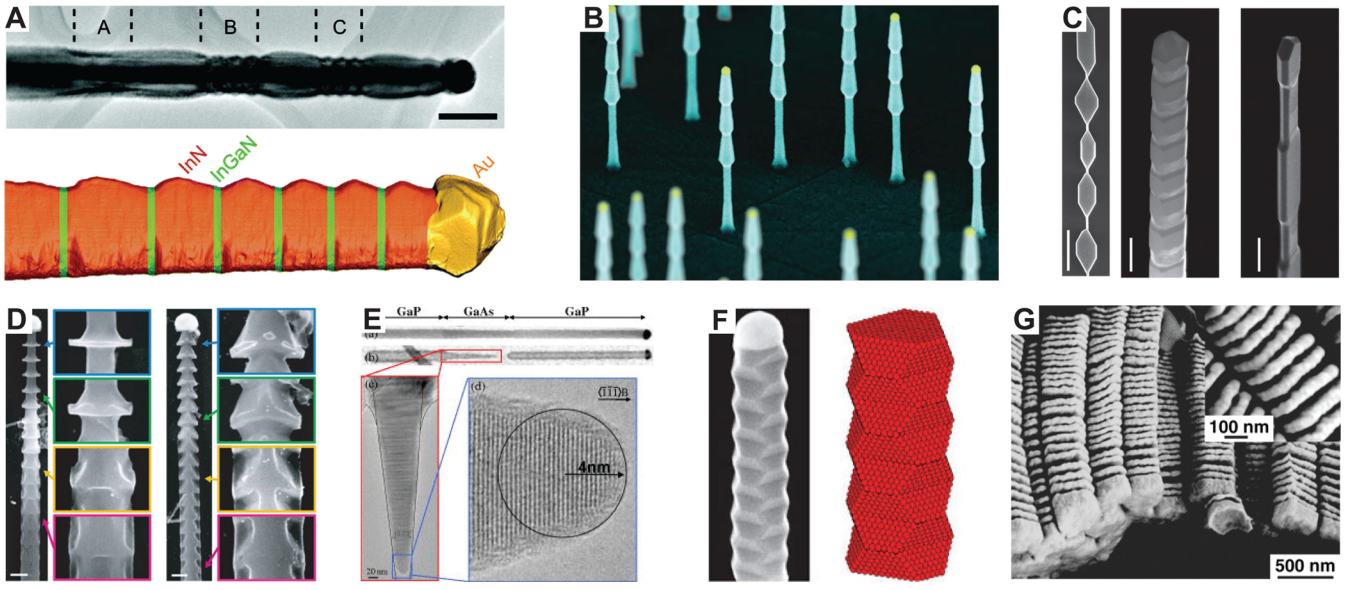

Figure 2. Methods for bottom-up control of NW morphology. (A) Diameter modulation of III–V VLS-grown NWs; scale bar, 100 nm. Images adapted from ref 14. Copyright 2013 American Chemical Society. (B) Chemically controlled vapor–solid sidewall deposition on Ge NWs. Reprinted with permission from ref 17. Copyright 2013, American Vacuum Society. (C) High-temperature shell deposition on Si NWs showing periodicity as a result of Plateau–Raleigh instability; scale bars, 400 nm. Adapted with permission from ref 12. Copyright 2015 Macmillan Publishers Ltd. (D) Si NWs with Au silicide that acts as an etch stop for aqueous KOH etching; scale bars, 200 nm. Reprinted with permission from ref 11. Copyright 2015 AAAS. (E) GaAs/GaP NWs etched in aqueous KOH solution. Reprinted with permission from ref 18. Copyright 2010 American Vacuum Society. (F) Twinning superlattice in InP NWs. Adapted with permission from ref 23. Copyright 2008 Macmillan Publishers Ltd. (G) Au NWs with gaps produced by on-wire lithography (OWL). Reprinted with permission from ref 24. Copyright 2005 AAAS.

deposition into a porous substrate, and the deposited material can be altered during growth. Following growth, the porous substrate is removed and the material is etched, leaving gaps less than 5 nm in length. Other template-assisted growth mechanisms, such as coaxial lithography[25] (COAL) and template-assisted selective epitaxy[26] (TASE), have also been developed to create complex structures.

In this Perspective, we highlight our recent efforts to encode morphologies with nanometer resolution in Si NWs, as illustrated in Figure 3, using the process we term ENGRAVE

DOI: 10.1021/acs.jpclett.5b02444
J. Phys. Chem. Lett. 2016, 7, 685–692

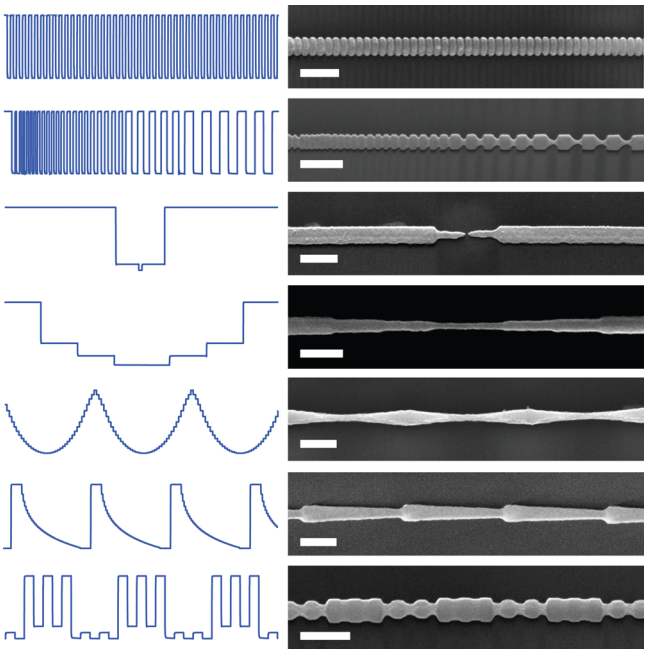

Figure 3. Gallery of ENGRAVE structures. The phosphine flow profile used to encode each morphology is shown as the blue curve to the left of each SEM image. All scale bars are 200 nm. Images adapted from ref 27. Copyright 2013 American Chemical Society.

(Encoded Nanowire GRowth and Appearance through VLS and Etching).[27−30] We outline the possibility of using NW morphology as a route to encode specific physical properties, including optical, electronic, biological, and thermal characteristics. In addition, we discuss the prospect for this process to become a complementary method for bottom-up yet lithographic-like patterning of semiconductors for a range of technological applications.

ENGRAVE can produce patterns that range from periodic, centrosymmetric to nonperiodic, asymmetric structures, including gratings, fractals, tapers, ratchets, sinusoids, nanogaps, and nanodots.

ENGRAVE works through precise control of phosphorus (P) dopant incorporation into VLS-grown Si NWs and through dopant-dependent, wet-chemical etching of the NWs in aqueous solution. The energy dispersive X-ray spectroscopy (EDS) image in Figure 4A, collected by a Tecnai Osiris scanning transmission electron microscopy (STEM) instrument, shows a Si NW encoded with n-type and nominally intrinsic sections, corresponding to areas of high and low P counts, respectively. The corresponding SEM image (Figure 4A) shows the same encoded section after a wet-chemical etch in aqueous KOH solution and illustrates how areas with high P doping levels act as an etch stop. The images also demonstrate that the P is confined to specific locations within the NW with abrupt transitions when the P concentration is changed. The incorporated P directly corresponds to the time periods of phosphine (PH_3) flow during

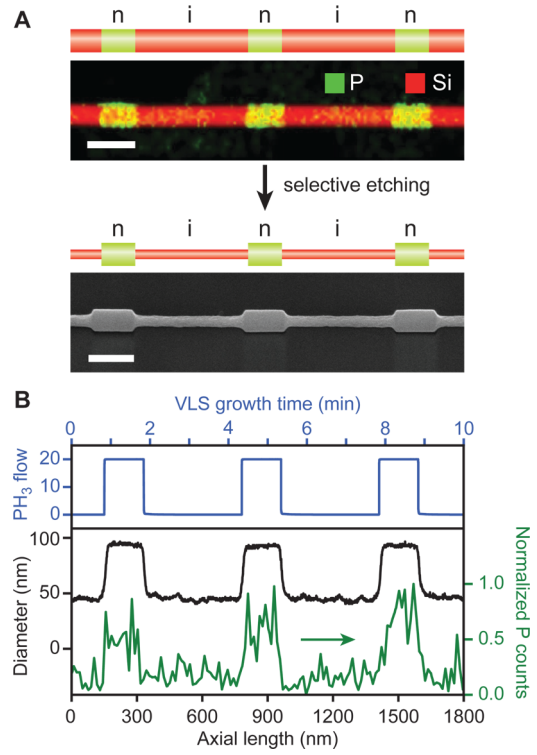

Figure 4. Fundamentals of Si NW doping. (A) Upper panel: Schematic of a Si NW with intrinsic (i) sections depicted in red and P-doped, n-type (n) sections depicted in green along with a STEM EDS image of a Si NW showing P counts in green and Si counts in red; scale bar, 200 nm. Lower panel: Schematic and SEM image of Si NW after wet-chemical KOH etching; scale bar, 200 nm. (B) Upper panel: PH_3 flow profile (in units of standard cubic centimeters per minute, sccm) during VLS growth of the NWs shown in panel A. Lower panel: Diameter profile (black curve and left-hand axis) derived from the SEM image in panel A and P signal (green curve and right-hand axis) derived from the EDS image in panel A. All images adapted from ref 30. Copyright 2014 American Chemical Society.

synthesis, as illustrated by the PH_3 flow, P EDS signal, and diameter profiles in Figure 4B.

To create precise sub-10 nm morphology, it is necessary to fully understand and characterize the NW growth rate and to optimize the abruptness of transitions from heavily doped n-type regions to nominally intrinsic regions. By using ENGRAVE as an analytical tool to probe the effects of various VLS growth parameters (temperatures, partial pressures, and total pressure) during synthesis by chemical vapor deposition (CVD), we have found conditions that produce uniform, diameter-independent growth rates[28] and ∼5 nm transitions between doped regions.[30] The growth rate of NWs is known to depend on wire diameter because of the Gibbs−Thomson effect,[31] which increases the vapor pressure of Si in the liquid catalyst of smaller diameter wires. By constructing a model of NW growth including the microscopic processes of Si incorporation, evaporation, and crystallization (Figure 5A), we found that the diameter dependence of wire growth rates is consistent with a diameter-dependent rate of Si evaporation from the liquid catalyst. We identified growth conditions in which the rate of Si evaporation is not a rate-limiting step for wire growth; as a result, the growth rate is diameter-independent in this regime. This growth regime is used for the ENGRAVE process to produce uniform features across all diameters of NWs in a sample.

DOI: 10.1021/acs.jpclett.5b02444
J. Phys. Chem. Lett. 2016, 7, 685−692

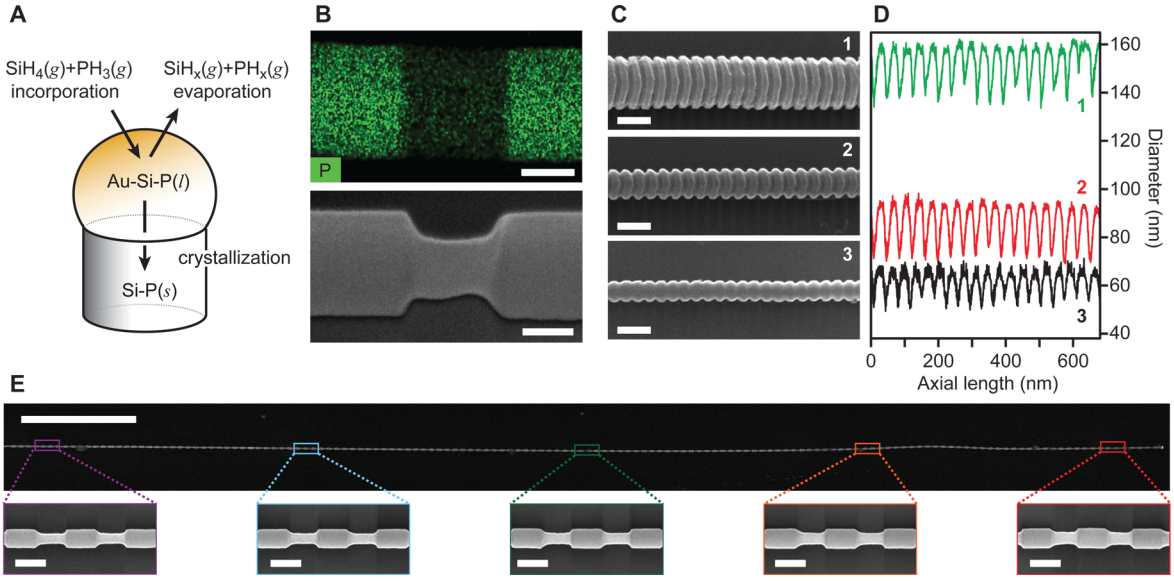

Figure 5. Diameter-independent growth rates and dopant transitions. (A) Illustration of the three key processes, incorporation, evaporation, and crystallization, that are used to model Si NW growth by the VLS mechanism. (B) EDS (top), showing P counts in green, and SEM (bottom) image of a NW grown under identical conditions after wet-chemical KOH etching; scale bars, 50 nm. (C) SEM images of ENGRAVE NWs created by alternating n-type/intrinsic sections for 6 s each. From top to bottom the NW diameters are (1) ~150 nm, (2) ~100 nm, and (3) ~50 nm; scale bars, 100 nm. (D) Diameter profiles as a function of axial length for NWs 1−3 shown in panel C. (E) Upper panel: SEM image of a grating-encoded NW more than 50 μm in axial length; scale bar, 5 μm. Lower panel: Higher-magnification SEM images of select sections of the NW in the upper panel; scale bars, 200 nm. All images adapted from refs 27 and 30. Copyright 2013 and 2014 American Chemical Society.

It was generally believed that the abruptness of heterostructures in a VLS-grown NW would be limited by a phenomena termed the "reservoir effect," in which material is retained in the liquid catalyst even after the gas-phase precursor for the material is removed, broadening transitions.[20,32,33] Using a kinetic model, as illustrated in Figure 5A, that includes P incorporation and evaporation from the catalyst and crystallization in the NW, we determined that the reservoir effect could by fully suppressed if the rate of P evaporation exceeds the rate of P crystallization.[30] We identified CVD growth parameters that satisfy this condition, and, as shown in Figure 5B, dopant transitions less than ~5 nm in width can be encoded. In addition, the dopants are uniformly distributed throughout the cross section of the wire. In combination with the diameter-independent growth rates, abrupt morphology can be encoded in wires of arbitrary diameter in a single growth, as illustrated in Figure 5C,D. In addition, this morphology can be encoded with fidelity over lengths greater than 50 μm (Figure 5E).

In combination with the diameter-independent growth rates, abrupt morphology can be encoded in wires of arbitrary diameter in a single growth, and this morphology can be encoded with fidelity over lengths greater than 50 μm.

Following VLS growth, ENGRAVE NWs are purely cylindrical, and the encoded morphology is revealed using aqueous solutions that selectively etch the wires based on the encoded doping level. Although there are many well-studied etchants for Si,[34] two of the most common are aqueous KOH and buffered hydrofluoric acid (BHF). With increasing doping level, the etch rate of Si is known to decrease for KOH whereas it is known to increase for BHF. As shown in panels A and B of Figure 6 for KOH and BHF, respectively, the two etchants have opposing etch rates versus doping level. The KOH etch, despite having an etch rate that is dependent on Si crystal direction,[35] produces a NW structure that is smooth and conformal with a surface roughness of ~0.5 nm, as shown in the AFM image in Figure 6C. We do not observe a crystallographic-dependent etch rate, and we suspect that the absence of an anisotropic etch is due to the cylindrical geometry of the NWs and the lack of well-defined crystal facets on the wire surface. The BHF etch, which has previously been demonstrated in similar modulation-doped Si NWs by the Filler group,[36] produces a slightly more abrupt morphology with the trade-off of a rougher and more porous surface. Although the porous structure can be desirable for some applications,[37] it can also be removed by performing multiple BHF etch steps with a mild oxidation of the porous regions between each step. Most importantly, the ability to quantify the etch rate versus doping level, combined with the uniform NW growth rates, allows the rational design of morphology in the NW using either etchant, as outlined in Figure 6D. This process involves (1) design of the NW structure, (2) determination of phosphine flow rates based on the measured etch rate, (3) growth of the NW using the calculated flow rates, and (4) a timed wet-chemical etch to fully realize the designed morphology. Using this strategy, we created bow-tie structures using both a KOH etch (Figure 6E) and a BHF etch (Figure 6F). The flow profiles for the two etchants are inverted (bottom panels of Figure 6E,F) yet produce qualitatively similar morphologies.

As an additional method of morphological control, the ENGRAVE NWs can be thermally oxidized. As shown by SEM images and diameter profiles before and after thermal oxidation (Figure 7A,B), the volumetric expansion of the NW caused by the lattice expansion from Si to SiO_2 results in a broadening of

DOI: 10.1021/acs.jpclett.5b02444
J. Phys. Chem. Lett. 2016, 7, 685−692

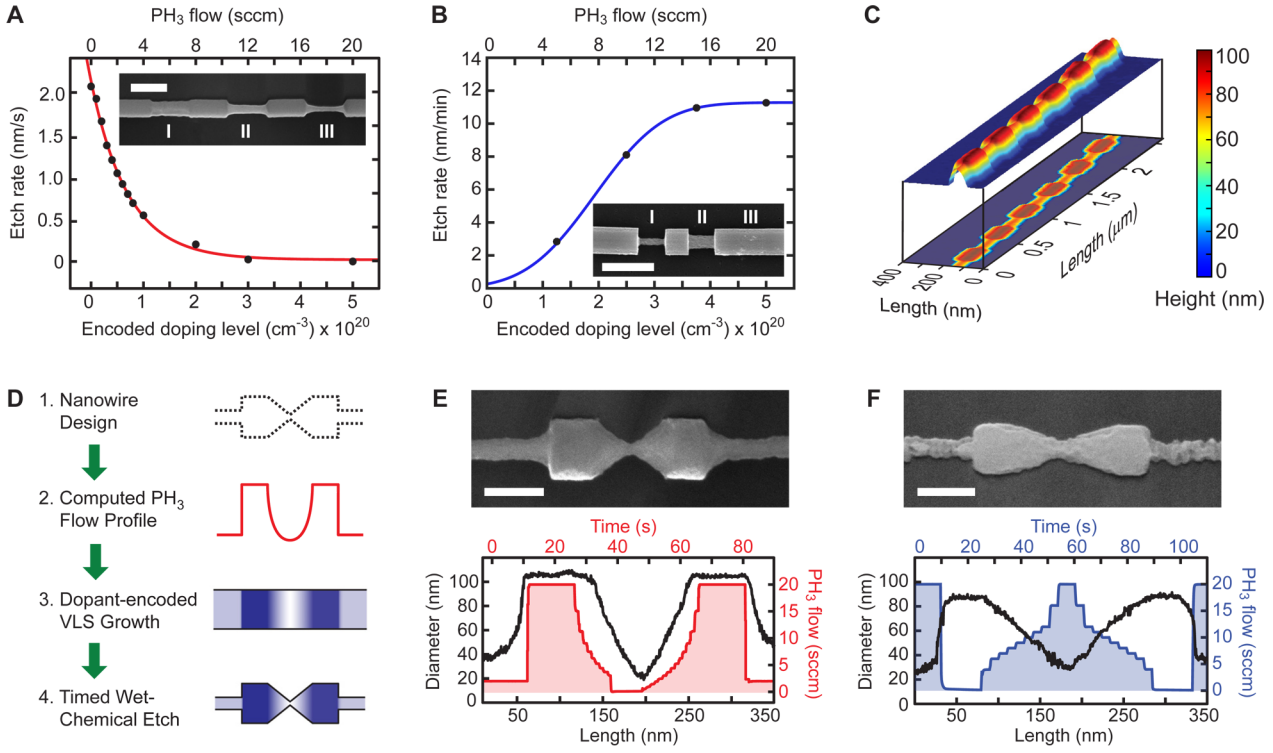

Figure 6. ENGRAVE process. (A) Radial etch rate of Si NWs in KOH as a function of encoded P doping levels. Red curve represents the best fit to a single-exponential function. Inset: SEM image of a NW with segments I, II, and III encoded with P doping levels of 1×10^{20} cm^{-3}, 5×10^{19} cm^{-3}, and intrinsic, respectively, and etched for 25 s; scale bar, 200 nm. (B) Radial etch rate of Si NWs in BHF as a function of encoded P doping levels. Blue curve represents the best fit to an error function. Inset: SEM image of a NW with segments I, II, and III encoded with P doping levels of 5×10^{20} cm^{-3}, 2.5×10^{20} cm^{-3}, and 1×10^{20} cm^{-3}, respectively, and etched for 8 min; scale bar, 200 nm. (C) AFM map of a NW grating etched with KOH. (D) Schematic of the sequential process for bottom-up synthesis of complex NW morphologies. (E) Upper panel: SEM image of a KOH-etched NW encoded with a bow-tie; scale bar, 100 nm. Lower panel: NW diameter (black curve and left-hand axis) as a function of length for the bow-tie shown in upper panel and measured phosphine flow rate (red curve and right-hand axis) in standard cubic centimeters per minute (sccm) as a function of time during CVD growth. (F) Upper panel: SEM image of a BHF-etched NW encoded with a bow-tie; scale bar, 100 nm. Lower panel: NW diameter (black curve and left-hand axis) as a function of length for the bow-tie shown in upper panel and measured phosphine flow rate (blue curve and right-hand axis) in sccm as a function of time during CVD growth. Images in panels A, D, and E adapted from ref 27. Copyright 2013 American Chemical Society.

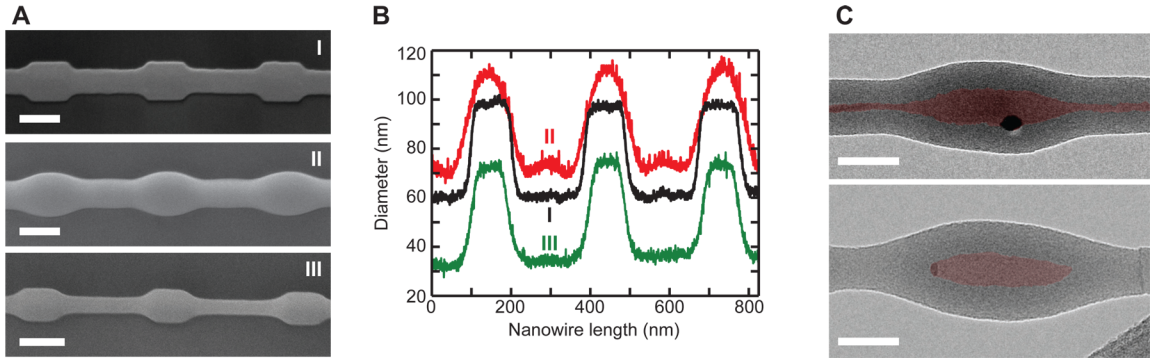

Figure 7. Thermal oxidation of ENGRAVE structures. (A) SEM images of a single ENGRAVE NW before (top; I) and after (middle; II) thermal oxidation and after removal of the thermal oxide (bottom; III); scale bars, 100 nm. (B) Diameter profiles derived from the SEM images in panel A before (black; I) and after (red; II) thermal oxidation and after removal of the thermal oxide (green; III). (C) False-color TEM images of etched NWs after thermal oxidation, in which the entire Si core (shaded red) retains its morphology (top) or the intrinsic segments are fully oxidized (bottom) leaving an ellipsoidal Si nanodot (shaded red); scale bars, 50 nm.

the outer shape. However, the Si core retains its morphology, which can be verified by removing the thermal oxide using a BHF etch (bottom panel in Figure 7A). Bright-field TEM imaging of a NW with more extensive thermal oxidation (Figure 7C) shows that the center of the NW corresponds to the crystalline Si core, which is surrounded by an oxide shell. It is also possible to completely oxidize the etched regions of the NWs, leaving behind isolated Si segments, ellipsoidal dots, as shown by the lower TEM image in Figure 7C. Oxidation of n-type doped Si is also known to drive dopants to the Si/SiO_2 interface because of electrostatic effects combined with the increased diffusion of dopants at elevated temperatures.[38−41] Thus, thermal oxidation can also be a route to remove dopants from the NWs, decoupling

DOI: 10.1021/acs.jpclett.5b02444
J. Phys. Chem. Lett. 2016, 7, 685−692

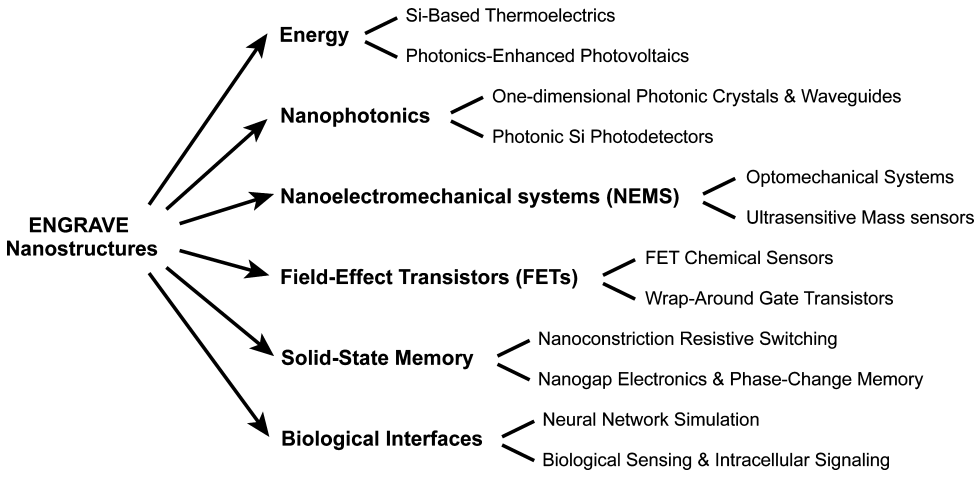

Figure 8. ENGRAVE technologies. Illustration of the broad set of technological applications that could be explored using morphology encoded through the ENGRAVE process.

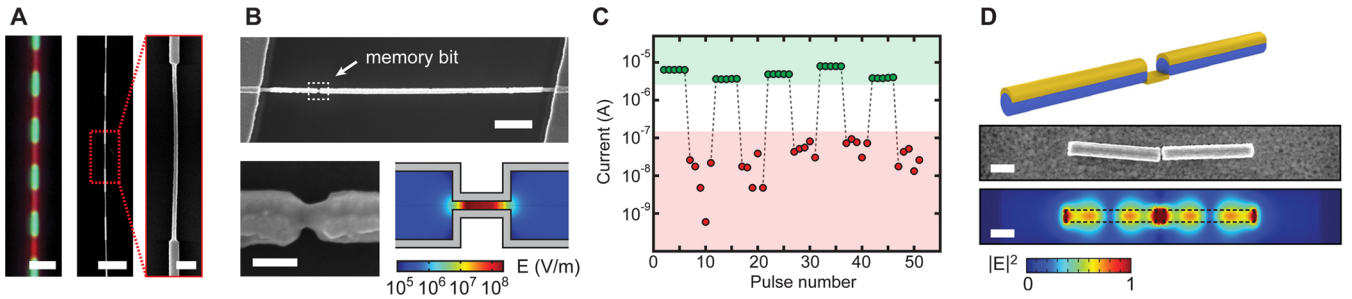

Figure 9. Demonstrated technologies enabled by the ENGRAVE process. (A) Dark-field microscopy image (left) and SEM image (middle and right) of a Si NW with 100 nm (green) and 50 nm (red) diameter segments; scale bars, 2 μm (left and middle) and 100 nm (right). (B) Upper panel: SEM image of a NW device encoded with a nonvolatile memory bit (dashed box) showing Ti/Pd Ohmic contacts on the far left and right; scale bar, 1 μm. Lower left: SEM image of the encoded memory bit corresponding to the dashed white box in panel B; scale bar, 100 nm. Lower right: finite-element simulation of the electric field magnitude across the NW at an applied bias of 8 V plotted in a logarithmic color scale for a nanorod segment 50 nm in length and 10 nm in diameter. (C) Resistive switching behavior over 10 memory cycles. Dashed lines represent the set/reset pulses between current readings, which were acquired five times at 1 V between each set or reset pulse. (D) Upper panel: Schematic illustration of Au deposition on a nanogap-encoded NW. Middle panel: SEM image of nanogap-encoded Si NW with 50 nm Au, gap of ~30 nm, and segment length of ~775 nm; scale bars, 200 nm. Lower panel: Finite-element optical simulations of the Si/Au nanogap structure above showing the scattered field ($|E|^2$) in the plane above the NW resulting from illumination at normal incidence with a transverse-magnetic plane wave at 633 nm; scale bar, 200 nm. Images in panels B, C, and D adapted from ref 27. Copyright 2013 American Chemical Society.

the connection between doping level, Fermi level, and morphology.

With these techniques for creating NWs with complex morphology, we can focus on the application of ENGRAVE to specific technologies, as illustrated schematically in Figure 8. Although this work is still in an early stage, we envision a broad set of possible technological applications in areas including energy, nanophotonics, nanoelectromechanical systems, field-effect transistors, solid-state memory, and biological interfaces,[11] among others, where the ability to connect many complex, independent, and even anisotropic structures could enable applications not achievable through other fabrication methods. For instance, the complex morphologies shown in Figure 3 could be used for a variety of technologies: suspended segments can be used as mechanical oscillators for nanoelectromechanical systems,[42] sawtooth segments can be used as electronic ratchets,[43] periodic gratings as optical elements in nanophotonic applications,[44,45] and nonperiodic gratings as a method to control thermal diffusion and enable thermoelectrics.[46] Several applications of ENGRAVE NWs have already been demonstrated, as shown in Figure 9. In the area of photonics, confining and manipulating light on the nanoscale is a key goal,[1,2] and we can precisely tune the properties of the NW to facilitate enhanced control of light at subwavelength dimensions.[29] The scattering of the NWs is strongly correlated with diameter, as shown in optical dark-field and SEM images in Figure 9A, where the smaller diameter segments scatter primarily red light and the larger diameters scatter primarily green light.

> We envision a broad set of possible technological applications in which the ability to connect many complex, independent, and even anisotropic structures could enable applications not achievable through other fabrication methods.

In addition to photonic applications, morphological changes can lead to electronic device applications such as nonvolatile memory.[27] Nonvolatile memory is a promising form of memory

DOI: 10.1021/acs.jpclett.5b02444
J. Phys. Chem. Lett. 2016, 7, 685−692

because it allows for fast, two-terminal reads and writes without need of a power supply to maintain the memory state.[47] To create a nonvolatile memory bit, we etched and thermally oxidized an ∼50 nm long intrinsic region to a diameter of ∼10 nm, as shown by the SEM image in Figure 9B. The geometry concentrates the voltage drop (see simulation in Figure 9B), which enhances the switching behavior. We fabricated Ohmic metal contacts to the n-type sections adjacent to the bit to apply voltage pulses and switch the resistivity. The bit can be repeatedly switched and obtains "on/off" current ratios of over 2 orders of magnitude (Figure 9C).

ENGRAVE NWs can also be used as a scaffold or template for other materials. To demonstrate this concept, NWs were grown with finely controlled n-type segments separated by a 50 nm gap (Figure 9D). We evaporated Au onto the gapped structure to create a plasmonic antenna. On the basis of simulations shown in Figure 9D, we tuned the length of the n-type segments to concentrate the electric field in the gap at a fixed wavelength, and the predicted field enhancement was directly mapped using surfaced enhanced Raman spectroscopy (SERS).[27]

Using materials beyond P-doped Si to produce ENGRAVE structures would open the door to new applications. Boron (B) doped Si, as well as germanium (Ge) doped Si and Si−Ge alloys, have been shown to act as an etch stop in KOH.[48] In particular, we expect that the ENGRAVE process can easily be extended to B-doped Si NWs; however, a new set of growth conditions will be needed to avoid deleterious vapor−solid deposition on the wire surface[49,50] and to achieve sufficiently high doping levels given the relatively lower incorporation rate of B in VLS-grown Si NWs.[51,52] The development of p-type ENGRAVE would allow the creation of p−n junctions with complex morphology, enabling new optoelectronic functionality. Beyond group IV NWs, III−V NWs have also been shown to have various etch rates depending on group V materials. For example, in a bromine wet etch, GaAs has an etch rate that is about 50 times greater than that of GaP, enabling morphological control.[18] Development of the ENGRAVE process with III−V materials could enable the design of photonic structures that take advantage of the direct bandgap of many III−V material systems.

In this Perspective, we have presented a new bottom-up method for controlling nanoscale morphology termed ENGRAVE. We have optimized both the growth and etching of ENGRAVE NWs to produce a range of abrupt and structurally varied NWs, and while ENGRAVE has been shown specifically in Si NWs, this research and process can potentially be applied to other NW systems. We presented a few simple examples of how ENGRAVE can be used in applications, yet there still remains a wealth of possible applications in which the structural control enabled by ENGRAVE could be a powerful method to create rationally designed structures. The high spatial resolution and flexibility afforded by the ENGRAVE process make it an exciting method to explore the connection between nanoscale morphology, physical properties, and technological applications.

AUTHOR INFORMATION

Corresponding Author

*E-mail: jfcahoon@unc.edu.

Notes

The authors declare no competing financial interest.

Biographies

Joseph D. Christesen received a B.S. in Chemistry and Computer Science from the College of William and Mary in 2011. He is currently a Ph.D. candidate in Chemistry at UNC-Chapel Hill, where he studies fundamental parameters of NW growth to synthesize shape-controlled NW structures for technological applications in James Cahoon's group.

Christopher W. Pinion received a B.S. in Chemistry and Physics from the University of South Carolina in 2012. He is currently pursuing his Ph.D. in Chemistry at UNC-Chapel Hill under the guidance of James Cahoon, with whom he examines the precise control of axial NW heterostructures.

David J. Hill is a graduate of the College of William and Mary, receiving a B.S. in Chemistry in 2013. As a Ph.D. candidate in the Cahoon group at UNC-Chapel Hill, he studies the optical properties of shape-controlled Si NWs.

Seokhyoung Kim graduated from Pohang University of Science and Technology (POSTECH) in chemistry in 2012 and received his M.S. in polymer science and engineering from the University of Massachusetts at Amherst in 2013. He is currently a Ph.D. student at UNC-Chapel Hill under the guidance of Professor James Cahoon and is working on preparation and characterization of single-NW photonic crystals.

James F. Cahoon received his B.S. in Chemistry and Philosophy from the College of William and Mary in 2003 and his Ph.D. in Physical Chemistry from UC-Berkeley in 2008, where he worked in the field of ultrafast vibrational spectroscopy with Charles Harris. Beginning in 2009, he worked as an I.C. postdoctoral fellow with Charles Lieber at Harvard University, and he began his independent career at UNC-Chapel Hill in 2011. His group combines synthetic control of semiconductor nanomaterials with detailed physical characterization and modeling to rationally design new functional materials. Webpage: http://cahoon.chem.unc.edu.

ACKNOWLEDGMENTS

We acknowledge primary support of this research by the National Science Foundation (NSF) through Grant DMR-1308695. C.W.P. and D.J.H. acknowledge NSF graduate research fellowships. S.K. acknowledges a Kwanjeong scholarship, and J.F.C. acknowledges a Packard Fellowship for Science and Engineering. We thank the staff of the Chapel Hill Analytical and Nanofabrication Laboratory (CHANL) user facility, especially Amar Kumbhar, for assistance with NW imaging.

REFERENCES

(1) Leung, S.-F.; Zhang, Q.; Xiu, F.; Yu, D.; Ho, J. C.; Li, D.; Fan, Z. Light Management with Nanostructures for Optoelectronic Devices. *J. Phys. Chem. Lett.* **2014**, *5*, 1479−1495.

(2) Koenderink, A. F.; Alù, A.; Polman, A. Nanophotonics: Shrinking Light-Based Technology. *Science* **2015**, *348*, 516−521.

(3) Maragò, O.; Jones, P.; Gucciardi, P.; Volpe, G.; Ferrari, A. C. Optical Trapping and Manipulation of Nanostructures. *Nat. Nanotechnol.* **2013**, *8*, 807−819.

(4) Ramos, D.; Gil-Santos, E.; Pini, V.; Llorens, J. M.; Fernández-Regúlez, M.; San Paulo, Á.; Calleja, M.; Tamayo, J. Optomechanics with Silicon Nanowires by Harnessing Confined Electromagnetic Modes. *Nano Lett.* **2012**, *12*, 932−937.

(5) Novotny, L.; van Hulst, N. Antennas for Light. *Nat. Photonics* **2011**, *5*, 83−90.

(6) Deotare, P. B.; McCutcheon, M. W.; Frank, I. W.; Khan, M.; Lončar, M. High Quality Factor Photonic Crystal Nanobeam Cavities. *Appl. Phys. Lett.* **2009**, *94*, 121106.

(7) International Technology Roadmap for Semiconductors, 2013 ed. http://itrs.net/.

(8) Chen, J.; Lim, B.; Lee, E. P.; Xia, Y. Shape-Controlled Synthesis of Platinum Nanocrystals for Catalytic and Electrocatalytic Applications. *Nano Today* **2009**, *4*, 81−95.

DOI: 10.1021/acs.jpclett.5b02444
J. Phys. Chem. Lett. 2016, 7, 685−692

(9) Tao, A. R.; Habas, S.; Yang, P. Shape Control of Colloidal Metal Nanocrystals. *Small* **2008**, *4*, 310−325.
(10) Halas, N. J. Plasmonics: An Emerging Field Fostered by Nano Letters. *Nano Lett.* **2010**, *10*, 3816−3822.
(11) Luo, Z.; Jiang, Y.; Myers, B. D.; Isheim, D.; Wu, J.; Zimmerman, J. F.; Wang, Z.; Li, Q.; Wang, Y.; Chen, X.; et al. Atomic Gold−enabled Three-Dimensional Lithography for Silicon Mesostructures. *Science* **2015**, *348*, 1451−1455.
(12) Day, R. W.; Mankin, M. N.; Gao, R.; No, Y.-S.; Kim, S.-K.; Bell, D. C.; Park, H.-G.; Lieber, C. M. Plateau−Rayleigh Crystal Growth of Periodic Shells on One-Dimensional Substrates. *Nat. Nanotechnol.* **2015**, *10*, 345−352.
(13) Musin, I. R.; Shin, N.; Filler, M. A. Diameter Modulation as a Route to Probe the Vapour−Liquid−Solid Growth Kinetics of Semiconductor Nanowires. *J. Mater. Chem. C* **2014**, *2*, 3285−3291.
(14) Lim, S.; Crawford, S.; Haberfehlner, G.; Gradečak, S. Controlled Modulation of Diameter and Composition along Individual III−V Nitride Nanowires. *Nano Lett.* **2013**, *13*, 331−336.
(15) Crawford, S.; Lim, S. K.; Gradecak, S. Fundamental Insights into Nanowire Diameter Modulation and the Liquid/Solid Interface. *Nano Lett.* **2013**, *13*, 226−232.
(16) Ma, Z.; McDowell, D.; Panaitescu, E.; Davydov, A. V.; Upmanyu, M.; Menon, L. Vapor−Liquid−Solid Growth of Serrated GaN Nanowires: Shape Selection Driven by Kinetic Frustration. *J. Mater. Chem. C* **2013**, *1*, 7294.
(17) Musin, I. R.; Boyuk, D. S.; Filler, M. a. Surface Chemistry Controlled Diameter-Modulated Semiconductor Nanowire Superstructures. *J. Vac. Sci. Technol. B* **2013**, *31*, 020603.
(18) Kallesøe, C.; Mølhave, K.; Larsen, K. F.; Engstrøm, D.; Hansen, T. M.; Bøggild, P.; Mårtensson, T.; Borgström, M.; Samuelson, L. Integration, Gap Formation, and Sharpening of III-V Heterostructure Nanowires by Selective Etching. *J. Vac. Sci. Technol. B* **2010**, *28*, 21.
(19) Fu, L.-T.; Chen, Z.-G.; Zou, J.; Cong, H.-T.; Lu, G.-Q. Fabrication and Visible Emission of Single-Crystal Diameter-Modulated Gallium Phosphide Nanochains. *J. Appl. Phys.* **2010**, *107*, 124321.
(20) Ross, F. M. Controlling Nanowire Structures Through Real Time Growth Studies. *Rep. Prog. Phys.* **2010**, *73*, 114501.
(21) Zeng, Z.; Li, Y.; Chen, J.; Zhou, W. GaP/GaO_x Core− Shell Nanowires and Nanochains and Their Transport Properties. *J. Phys. Chem. C* **2008**, *112*, 18588−18591.
(22) Ross, F. M.; Tersoff, J.; Reuter, M. C. Sawtooth Faceting in Silicon Nanowires. *Phys. Rev. Lett.* **2005**, *95*, 146104.
(23) Caroff, P.; Dick, K. a; Johansson, J.; Messing, M. E.; Deppert, K.; Samuelson, L. Controlled Polytypic and Twin-Plane Superlattices in III-V Nanowires. *Nat. Nanotechnol.* **2009**, *4*, 50−55.
(24) Qin, L.; Park, S.; Huang, L.; Mirkin, C. On-Wire Lithography. *Science* **2005**, *309*, 113−115.
(25) Ozel, T.; Bourret, G. R.; Mirkin, C. A. Coaxial Lithography. *Nat. Nanotechnol.* **2015**, *10*, 319−324.
(26) Schmid, H.; Borg, M.; Moselund, K.; Gignac, L.; Breslin, C. M.; Bruley, J.; Cutaia, D.; Riel, H. Template-Assisted Selective Epitaxy of III−V Nanoscale Devices for Co-Planar Heterogeneous Integration with Si. *Appl. Phys. Lett.* **2015**, *106*, 233101.
(27) Christesen, J. D.; Pinion, C. W.; Grumstrup, E. M.; Papanikolas, J. M.; Cahoon, J. F. Synthetically Encoding 10 nm Morphology in Silicon Nanowires. *Nano Lett.* **2013**, *13*, 6281−6286.
(28) Pinion, C. W.; Nenon, D. P.; Christesen, J. D.; Cahoon, J. F. Identifying Crystallization- and Incorporation-Limited Regimes during Vapor-Liquid-Solid Growth of Si Nanowires. *ACS Nano* **2014**, *8*, 6081−6088.
(29) Hill, D. J.; Pinion, C. W.; Christesen, J. D.; Cahoon, J. F. Waveguide Scattering Microscopy for Dark-Field Imaging and Spectroscopy of Photonic Nanostructures. *ACS Photonics* **2014**, *1*, 725−731.
(30) Christesen, J. D.; Pinion, C. W.; Zhang, X.; McBride, J. R.; Cahoon, J. F. Encoding Abrupt and Uniform Dopant Profiles in Vapor−Liquid−Solid Nanowires by Suppressing the Reservoir Effect of the Liquid Catalyst. *ACS Nano* **2014**, *8*, 11790−11798.
(31) Givargizov, E. I. Fundamental Aspects of VLS Growth. *J. Cryst. Growth* **1975**, *31*, 20−30.
(32) Wen, C. Y.; Reuter, M. C.; Bruley, J.; Tersoff, J.; Kodambaka, S.; Stach, E. A.; Ross, F. M. Formation of Compositionally Abrupt Axial Heterojunctions in Silicon-Germanium Nanowires. *Science* **2009**, *326*, 1247−1250.
(33) Dick, K.; Bolinsson, J.; Borg, B.; Johansson, J. Controlling the Abruptness of Axial Heterojunctions in III−V Nanowires: Beyond the Reservoir Effect. *Nano Lett.* **2012**, *12*, 3200−3206.
(34) Williams, K. R.; Muller, R. S. Etch Rates for Micromachining Processing. *J. Microelectromech. Syst.* **1996**, *5*, 256−269.
(35) Bean, K. E. Anisotropic Etching of Silicon. *IEEE Trans. Electron Devices* **1978**, *25*, 1185−1193.
(36) Chou, L.; Boyuk, D. S.; Filler, M. A. Optically Abrupt Localized Surface Plasmon Resonances in Si Nanowires by Mitigation of Carrier Density Gradients. *ACS Nano* **2015**, *9*, 1250−1256.
(37) Hochbaum, A. I.; Chen, R.; Delgado, R. D.; Liang, W.; Garnett, E. C.; Najarian, M.; Majumdar, A.; Yang, P. Enhanced Thermoelectric Performance of Rough Silicon Nanowires. *Nature* **2008**, *451*, 163−167.
(38) Johannessen, J. S.; Spicer, W. E.; Gibbons, J. F.; Plummer, J. D.; Taylor, N. J. Observation of Phosphorus Pile-up at the SiO_2-Si Interface. *J. Appl. Phys.* **1978**, *49*, 4453.
(39) Lau, F.; Mader, L.; Mazure, C.; Werner, C.; Orlowski, M. A Model for Phosphorus Segregation at the Silicon-Silicon Dioxide Interface. *Appl. Phys. A: Solids Surf.* **1989**, *49*, 671−675.
(40) Schmidt, V.; Senz, S.; Gösele, U. Influence of the Si/SiO_2 Interface on the Charge Carrier Density of Si Nanowires. *Appl. Phys. A: Mater. Sci. Process.* **2006**, *86*, 187−191.
(41) Kramer, N. J.; Schramke, K. S.; Kortshagen, U. R. Plasmonic Properties of Silicon Nanocrystals Doped with Boron and Phosphorus. *Nano Lett.* **2015**, *15*, 5597−5603.
(42) Zhu, J.; Peng, H.; Chan, C. K.; Jarausch, K.; Zhang, X. F.; Cui, Y. Hyperbranched Lead Selenide Nanowire Networks. *Nano Lett.* **2007**, *7*, 1095−1099.
(43) Belinicher, V. I.; Sturman, B. I. The Photogalvanic Effect in Media Lacking a Center of Symmetry. *Usp. Fiz. Nauk* **1980**, *130*, 415.
(44) Van Laer, R.; Kuyken, B.; Van Thourhout, D.; Baets, R. Interaction between Light and Highly Confined Hypersound in a Silicon Photonic Nanowire. *Nat. Photonics* **2015**, *9*, 199−203.
(45) Fu, A.; Gao, H.; Petrov, P.; Yang, P. Widely Tunable Distributed Bragg Reflectors Integrated into Nanowire Waveguides. *Nano Lett.* **2015**, *15*, 6909−6913.
(46) Zianni, X. Diameter-Modulated Nanowires as Candidates for High Thermoelectric Energy Conversion Efficiency. *Appl. Phys. Lett.* **2010**, *97*, 233106.
(47) Waser, R.; Aono, M. Nanoionics-Based Resistive Switching Memories. *Nat. Mater.* **2007**, *6*, 833−840.
(48) Palik, E. D.; Bermudez, V. M.; Glembocki, O. J. Ellipsometric Study of the Etch-Stop Mechanism in Heavily Doped Silicon. *Solid-State Electron.* **1985**, *28*, 209.
(49) Gentile, P.; Solanki, a; Pauc, N.; Oehler, F.; Salem, B.; Rosaz, G.; Baron, T.; Den Hertog, M.; Calvo, V. Effect of HCl on the Doping and Shape Control of Silicon Nanowires. *Nanotechnology* **2012**, *23*, 215702.
(50) Pan, L.; Lew, K.-K.; Redwing, J. M.; Dickey, E. C. Effect of Diborane on the Microstructure of Boron-Doped Silicon Nanowires. *J. Cryst. Growth* **2005**, *277*, 428−436.
(51) Schlitz, R. A.; Perea, D. E.; Lensch-Falk, J. L.; Hemesath, E. R.; Lauhon, L. J. Correlating Dopant Distributions and Electrical Properties of Boron-Doped Silicon Nanowires. *Appl. Phys. Lett.* **2009**, *95*, 162101.
(52) Schmid, H.; Bessire, C.; Björk, M. T.; Schenk, A.; Riel, H. Silicon Nanowire Esaki Diodes. *Nano Lett.* **2012**, *12*, 699−703.

DOI: 10.1021/acs.jpclett.5b02444
J. Phys. Chem. Lett. 2016, 7, 685−692